THE JOURNAL OF PHYSICAL CHEMISTRY B

Article

pubs.acs.org/JPCB

Polarization-Sensitive Sum-Frequency Generation Microscopy of Collagen Fibers

Yang Han, Julie Hsu, Nien-Hui Ge, and Eric O. Potma*

Department of Chemistry, University of California at Irvine, Irvine, California 92697-2025, United States

Supporting Information

ABSTRACT: Point-scanning sum-frequency generation (SFG) microscopy enables the generation of images of collagen I fibers in tissues by tuning into specific vibrational resonances of the polypeptide. It is shown that when collagen-rich tissues are visualized near the 2954 cm^{-1} stretching vibration of methylene groups, the SFG image contrast is higher compared to the contrast seen in nonresonant second-harmonic generation (SHG) imaging. Polarization and spectrally resolved analysis of the SFG signal as a function of fiber orientation in the CH-stretching range of the vibrational spectrum enabled a comparative characterization of the achiral tensor elements of collagen's second-order susceptibility. This analysis reveals that selected on-resonance tensor elements are enhanced over other elements, giving rise to a much stronger anisotropy ρ of the signal for SFG ($\rho \approx 15$) compared to SHG ($\rho \approx 3$). The improved anisotropy of the vibrationally resonant signal contributes to the higher contrast seen in the SFG tissue images.

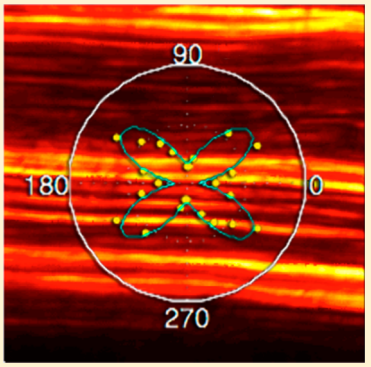

1. INTRODUCTION

Sum-frequency generation (SFG) spectroscopy is a nonlinear optical technique that probes the nonlinear response of materials, as described by the second-order susceptibility $\chi^{(2)}$. The technique uses two incident optical frequencies, ω_1 and ω_2, to generate a signal at the sum frequency $\omega_3 = \omega_1 + \omega_2$. SFG is useful for probing a special class of specimens: those that exhibit noncentrosymmetry over the length scale of the probing volume, which is a direct consequence of the spatial symmetry properties of $\chi^{(2)}$. Such conditions are inherently met at planar surfaces or in materials with an intrinsic noncentrosymmetric molecular ordering. Moreover, the SFG process can be enhanced when tuning one or both of the incident frequencies into resonance with a molecular mode. In vibrationally resonant SFG, ω_1 is in the mid-infrared range and used to drive specific vibrational modes. The combination of surface selectivity and vibrational spectroscopic sensitivity has rendered SFG a popular tool for studying molecular properties at interfaces.[1−4]

When SFG spectroscopy is performed under polarization resolved conditions, different elements of the $\chi^{(2)}_{ijk}$ tensor, where (i, j, k) indicate the polarization direction of the $(\omega_3, \omega_2, \omega_1)$ fields, can be independently characterized. Since the measured tensor elements are ultimately related to the hyperpolarizability of chemical group vibrations and their orientation with respect to the laboratory frame, polarization-sensitive SFG spectroscopy has been used extensively for relating the properties of chemical group vibrations to molecular orientation at interfaces. If the molecular mode vibrations are well-defined, information about the orientation of chemical groups at the interface can be extracted. Vice versa, if the molecular orientation is known, details on the mode properties can be acquired.[5,6]

Polarization-sensitive SFG spectroscopy is conventionally carried out with shallowly focused beams that illuminate an area of the order of 100 × 100 μm^2 from which the spatially averaged signal is collected. This macroscopic excitation and detection mode is not sensitive to spatial heterogeneities in the sample that manifest themselves on the (sub)micrometer scale. To resolve spatial variations in the sample on such length scales, SFG can be adopted for microscopic probing with the aid of high numerical aperture lenses. Various implementations of SFG microscopy have been realized, based on either a point- or widefield-illumination configuration.[7−12] These various forms of SFG microscopy have been used to study a growing number of spatially heterogeneous samples, including patterned molecular monolayers on planar surfaces,[7] biomolecular microcrystals,[13,14] and biofibers.[9,15,16]

Among the various forms of SFG microscopy, the point-scanning configuration with collinear excitation beams is attractive because the microscope layout is similar to a standard laser-scanning nonlinear optical microscope.[17] This configuration not only enables fast scanning capabilities with submicrometer lateral resolution, but also allows the simultaneous recording of images based on alternative forms of nonlinear optical contrast such as nonresonant second harmonic generation (SHG),[18] which is especially useful when imaging microscopic structures with intrinsic noncentrosymmetry. The flexibility of this multimodal nonlinear microscopy approach is further exemplified by the implementation of phase-sensitive SFG detection, allowing direct recordings of $\mathrm{Im}\{\chi^{(2)}\}$.[16] However, point-scanning SFG microscopy has not yet taken full advantage of the wealth of information available through polarization-sensitive detection.

Received: November 4, 2014
Revised: January 22, 2015
Published: January 23, 2015

DOI: 10.1021/jp511058b
J. Phys. Chem. B 2015, 119, 3356−3365

In this contribution, we describe the first polarization-resolved implementation of laser-scanning SFG microscopy. We show that the polarization-sensitive SFG microscope makes it possible to generate images with contrast based on various independent $\chi^{(2)}_{ijk}$ tensor elements. Compared to previous laser-scanning SFG studies, access to individual tensor elements enables a more advanced analysis of molecular orientation and offers additional contrast mechanisms for studying spatial heterogeneities in the sample. To demonstrate the new capabilities of this technique, we have chosen to examine the orientation of molecular modes in collagen fibrils in collagen-rich tissues. Known for their nonvanishing (bulk) $\chi^{(2)}$, collagen I fibrils have been extensively studied with nonresonant SHG microscopy,[19−23] polarization-sensitive SHG measurements,[24−26] as well as with macroscopic SFG spectroscopy.[27−30] Despite the widespread use of nonresonant SHG microscopy for visualizing collagen in biological tissues, the molecular origin of the nonresonant contrast remains unclear. Both electronic[31] and off-resonance vibrational modes[25] have been suggested to contribute to the observed collagen signal in SHG images. SFG microscopy is a suitable technique for adding important microspectroscopic information to the ongoing debate about the chemical origins of the optical nonlinearity of collagen.

Here we combine SHG microscopy directly with SFG microscopy for the visualization of collagen-rich tissues, and observe that under resonant conditions, the SFG image shows better contrast. The use of polarization-resolved SFG enables a more detailed look at the individual tensor elements that contribute to the signal. By studying the spectral properties of the tensor elements in the CH-stretching range of the vibrational spectrum, it is shown that the on-resonance SFG signal is carried by selected tensor elements of collagen. A subsequent investigation of the dependence of the SFG signal on the orientation of the tissue provides evidence for the presence of $\chi^{(2)}$-active tissue structures other than aligned collagen fibers. The study presented here demonstrates that the added analytical capabilities of polarization-resolved SFG offer valuable information regarding the molecular properties of $\chi^{(2)}$-active structures in the tissue, beyond what can be achieved with SHG microscopy alone.

2. EXPERIMENTAL METHODS

2.1. SFG Microscope. The polarization-sensitive SFG imaging platform is based on a collinear nonlinear optical microscope, which has been described before.[18] A sketch of the setup is shown in Figure 1. Briefly, the system uses the near-infrared (ω_2, tuned between 12 857 and 13 127 cm^{-1}) and mid-infrared (ω_1, tuned from 2835 to 2970 cm^{-1}) output of a picosecond optical parametric oscillator source with a pulse repetition rate of 76 MHz. The linear polarization orientation of each incident beam is controlled by independent half-wave plates and polarizers. The polarizer for the mid-infrared beam is a BaF_2 holographic wire grid polarizer (extinction ratio 150:1 at 3300 cm^{-1}) while the polarizer for the near-infrared beam is a SF2 polarizer (extinction ratio 1000:1). The two beams are combined collinearly on a dichroic mirror and directed to a microscope frame, which included a CaF_2 tube lens. The excitation beams are focused with a 0.65 NA reflective objective onto the sample. The SFG signal is captured by a refractive condenser lens in the forward direction and passed through a bandpass filter and analyzer before it is detected by a photomultiplier tube. The sample is mounted on a two-dimensional piezo-stage and raster scanned relative to the focal spot for generating the SFG images. The system can also be used for generating SHG images. For this purpose, the SHG signal induced by the ω_2 beam is captured sequentially by the same detection system by use of a different bandpass filter. The spectral resolution of the measurements is 6 cm^{-1}, as defined by the spectral width of the pulses.

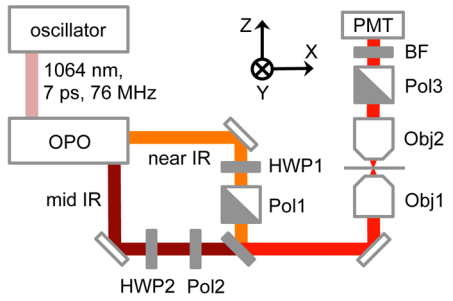

Figure 1. Schematics of the SFG microscope setup. The input power and polarization of near-IR and mid-IR beams are controlled by independent half wave plates (HWP 1 and 2) and polarizers (Pol 1 and 2). The excitation beams are focused by a microscope objective lens (Obj1) and the signal is collected by a second objective lens (Obj2) in the forward direction. The SFG signal passes through the analyzer (Pol 3) and bandpass filter (BF) and is detected by a photomultiplier tube (PMT).

2.2. Collagen Samples. We present images of two collagen-rich tissues: hawk cornea and rat tail tendon. Cornea samples consist of 100 μm thick sagittal slices from a hawk eye. The slices are gently laid on a glass coverslip and immersed in phosphate buffered saline. Rat tail tendon tissue is cut to 100 μm thick slices and flattened between two glass coverslips before SFG imaging.

2.3. Sample Configuration. The definition of the Cartesian coordinates is given in Figure 2. The laboratory-fixed frame is defined by the (X, Y, Z) coordinates, where (X, Y) forms the lateral plane and Z defines the axial coordinate, which constitutes the main light propagation axis. The collagen fiber-fixed frame is defined by (x, y, z), where the long axis of the fiber is aligned along the y coordinate, and (x, z) is the plane of rotational symmetry. A rotation of the fiber around Z is described by the angle ϕ, while a rotation around x is characterized by the angle θ. Rotations are in a clockwise fashion following the right-hand rule. The collagen fiber is assumed to have cylindrical symmetry with symmetry properties that belong to the $C_{\infty v}$ point group.[27] Under these

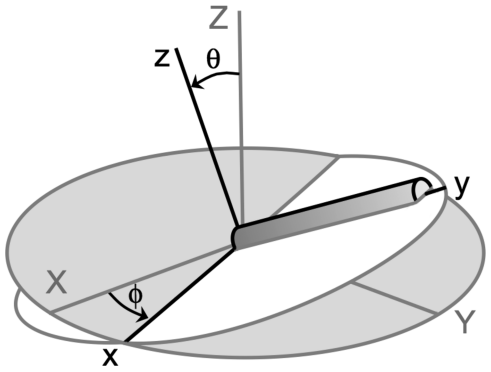

Figure 2. Orientation of the laboratory frame (X, Y, Z) and collagen fiber frame (x, y, z).

DOI: 10.1021/jp511058b
J. Phys. Chem. B 2015, 119, 3356−3365

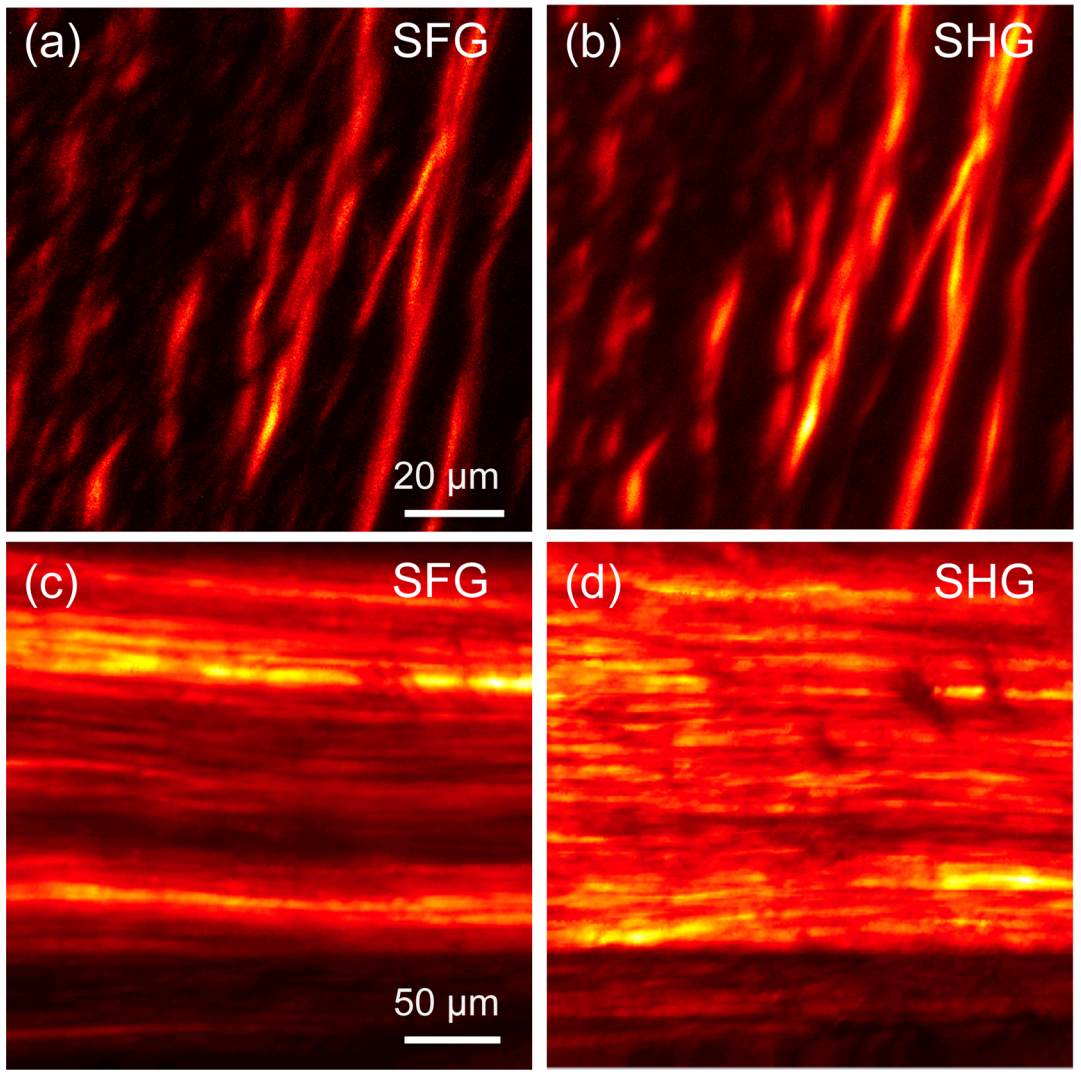

Figure 3. Normalized SFG (a) and SHG (b) images of hawk cornea and SFG (c) and SHG (d) images of rat tail tendon taken at ω_1= 2950 cm^{-1} and ω_2= 12 897 cm^{-1} with the polarization direction of both excitation beams aligned with the long axis of the main collagen structures.

assumptions, there are 7 nonzero achiral tensor elements ($\chi^{(2)}_{yyy}$, $\chi^{(2)}_{yzz} = \chi^{(2)}_{yxx}$, $\chi^{(2)}_{zzy} = \chi^{(2)}_{xxy}$, $\chi^{(2)}_{zyz} = \chi^{(2)}_{xyx}$) and 6 nonzero chiral tensor elements ($\chi^{(2)}_{zxy} = -\chi^{(2)}_{xzy}$, $\chi^{(2)}_{xyz} = -\chi^{(2)}_{zyx}$, $\chi^{(2)}_{yzx} = -\chi^{(2)}_{yxz}$) of the nonlinear susceptibility.

In the polarization-resolved experiments, the excitation beams are either *X*-polarized or *Y*-polarized when they are combined and directed toward the microscope. The sample is rotated to monitor the orientation dependence of the collagen fibers. Rotating the sample suppresses the introduction of elliptically polarized components that may otherwise arise at the dichroic beamsplitter when the polarization orientation of the beam is a combination of *X*- and *Y*-polarizations. At the back aperture of the objective lens, the polarization state of the incident beams is linear with an error margin less than 1%, predominately determined by the extinction ratio of the polarizer.

It is well-known that focusing a linearly polarized field with a high numerical objective produces orthogonal field components in the vicinity of the focal volume.[32] In our configuration of a 0.65 NA reflective lens, diffraction calculations indicate that illumination with *Y*-polarized incident light yields a ∼5% portion of light intensity polarized in the axial direction. Because the signal contributions originating from axial components of the focal field are below the noise of the experiments presented here, we assume in the analysis of the results that the *X*- and *Y*-polarized field components are the dominant contributions in focus and that contributions resulting from axial (Z) field components can be ignored.

Under these experimental conditions, assuming that the collagen fibers are mainly aligned in the (X, Y) plane, i.e. $\theta \approx 0$, the measurement is insensitive to tensor elements with *z*-indices. Therefore, the dominant tensor elements that describe the response of the collagen fiber probed in the SFG imaging experiments are the achiral elements $\chi^{(2)}_{yyy}$, $\chi^{(2)}_{yxx}$, $\chi^{(2)}_{xxy}$, and $\chi^{(2)}_{xyx}$. Note that in a corresponding SHG imaging experiment, the last two tensor elements are necessarily the same ($\chi^{(2)}_{xxy} = \chi^{(2)}_{xyx}$) since the last two indices of $\chi^{(2)}_{ijk}$ are interchangeable.

3. RESULTS

3.1. Combined SHG and SFG Imaging of Collagen. The SFG microscope is sensitive to the same spatial symmetries as conventional SHG microscopy, with the important exception that vibrationally resonant components of the nonlinear susceptibility can be specifically mapped out. Figure 3 shows SHG and SFG images of hawk cornea and rat tail tendon, both tissues rich in collagen I. For the SFG contrast, the ω_1 beam

DOI: 10.1021/jp511058b
J. Phys. Chem. B 2015, 119, 3356−3365

was tuned to the carbon−hydrogen stretching vibration near 2950 cm^{-1}. The polarization direction of both excitation beams is aligned with the long axis of the main collagen structures in the image, and no analyzer is used in the measurement. We note that under the experimental conditions used here the resonant SFG signal is between 2 and 5 times stronger than the nonresonant SHG signal. As is evident from the figure, the image contrast from collagen in both SFG and SHG modalities is largely similar, as both modalities are sensitive to similar tensor elements of $\chi^{(2)}$. Features seen in the SHG images are reproduced in the SFG images. Nonetheless, some differences can be observed as well. First, the lateral resolution in the SFG images is lower (0.65 μm for SFG versus 0.45 μm for SHG) because of the longer excitation wavelength of ω_1. Second, qualitatively, the contrast in the SFG images appears higher, with somewhat better defined fibrillar structures in the tendon tissue and lower signal contributions from parts of the tissue that are not aligned with the main axis of collagen fibers.

A possible explanation for the better contrast of the SFG signal is the higher anisotropy of the signal as a function of the orientation of the fiber. In nonresonant SHG imaging experiments of rat tail tendon, the signal is typically ~3 times higher when the linear polarization of both excitation beams is aligned with the long axis of the fiber compared to when it is orthogonal to the main fiber axis ($\rho = I_{\parallel}/I_{\perp} \approx 3$).[24,25,33] We find that the SFG signal from the collagen mode near 2950 cm^{-1} exhibits a much higher value for ρ. Figure 4a,b shows the marked differences between the SFG signals obtained when the excitation polarization is parallel or orthogonal to the long axis of the collagen fibers in rat tail tendon. Panels c and d in Figure 4 give the corresponding SHG images, which show a less significant difference between parallel and perpendicular polarization of the excitation beams. Figure 4e shows the measured values of ρ for different vibrational energies. For comparison, the ρ values of the SHG signal, measured from the same sample and under similar conditions of the pump wavelength, are indicated as well. Whereas the anisotropy of the SHG signal is constant with pump wavelength, the anisotropy of the SFG signal changes radically across this range of vibrational energies. The much higher anisotropy of the SFG signal implies that the SFG signal is more sensitive to fiber orientation. Hence, whenever there is a distribution of fiber orientations, the SFG signal is expected to yield higher contrast compared to the nonresonant SHG response.

Specifically, the SFG anisotropy grows to a ratio $\rho \approx 15$ when tuned into resonance with the band near 2950 cm^{-1}. This indicates that the relative contributions of the nonvanishing $\chi^{(2)}$ tensor elements change when the system is driven at a molecular resonance compared to when the molecule is addressed off-resonance. In the configuration here, $I_{\parallel}$ measures $\chi^{(2)}_{yyy}$ and $\chi^{(2)}_{xyy}$, whereas $I_{\perp}$ probes $\chi^{(2)}_{yxx}$ and $\chi^{(2)}_{xxx}$. If cylindrical symmetry of the collagen fiber is assumed, the ratio $I_{\parallel}/I_{\perp}$ can be recast as $|\chi^{(2)}_{yyy}/\chi^{(2)}_{yxx}|^2$. For the parallel beams used here, we conclude that the $|\chi^{(2)}_{yyy}/\chi^{(2)}_{yxx}|^2$ ratio near 2950 cm^{-1} is significantly higher than when the signal is measured off-resonance. Second, around 2910 cm^{-1}, a minimum of the SFG anisotropy is seen, where ρ dips below 1. This insinuates the presence of a resonance with an orthogonal polarization anisotropy. To gain more insight in the observed differences in resonant and nonresonant contrast, spectrally and polarization resolved studies were performed, which are discussed next.

3.2. Polarization-Resolved SFG of the Carbon−Hydrogen Stretching Mode. Using polarization-resolved SFG microscopy, it is possible to examine the spectral dependence of individual tensor elements. In Figure 5, the spectra of eight different tensor elements in the CH stretching range are shown. The spectra were taken from rat tail tendon, where the long axis of the collagen fibers is predominantly oriented along the *Y*-coordinate. In this configuration $\phi = 0$, the measured tensor element is expected to directly relate to the corresponding tensor element of the fiber, $\chi^{(2)}_{IJK} = \chi^{(2)}_{ijk}$. Assuming that cylindrical symmetry holds, we may expect nonzero contributions from the $\chi^{(2)}_{yyy}$, $\chi^{(2)}_{yxx}$, $\chi^{(2)}_{xxy}$, and $\chi^{(2)}_{xyx}$ elements. Figure 5a shows a strong resonance at 2954 cm^{-1} for the $\chi^{(2)}_{yyy}$ and $\chi^{(2)}_{xxy}$ elements. The 2954 cm^{-1} resonance is much weaker in the $\chi^{(2)}_{yxx}$ and $\chi^{(2)}_{xyx}$ elements. This implies that a strong resonance is seen only when the polarization of the ω_1 field is aligned with the long axis of the fiber.

Based on the molecular structure of collagen, which is composed predominantly of methylene-rich proline and glycine residues, the vibrational modes of methylene are likely contributors to the vibrational spectrum in the CH-stretching

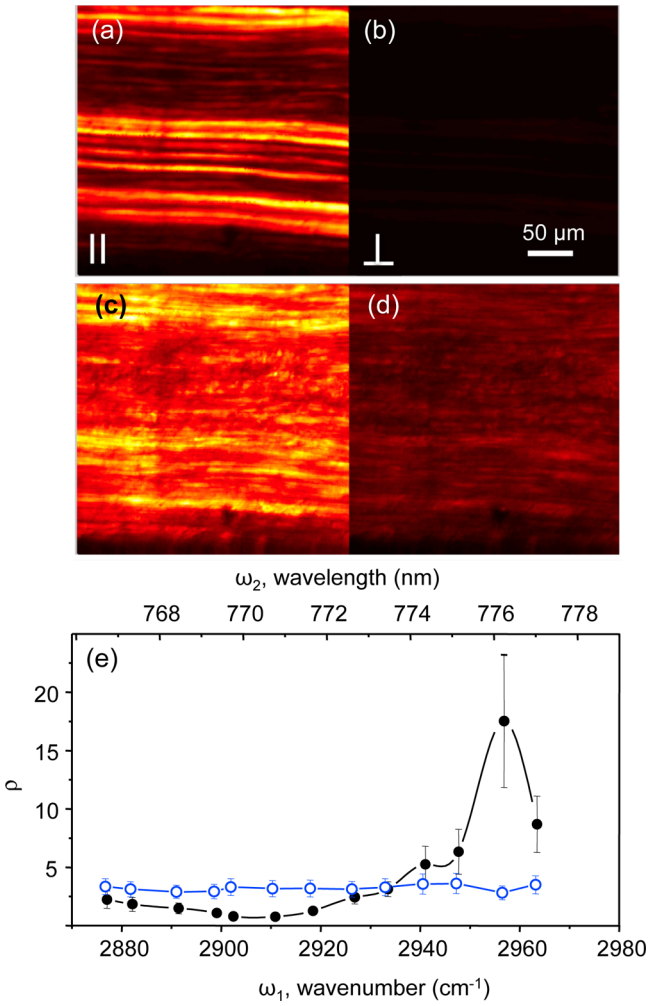

Figure 4. SFG signal measured with both incident beams polarized along the long axis of the fiber (a) and the SFG signal measured with the incident polarization orthogonal to the long axis of the fiber (b). Panels c and d show the SHG signal under identical polarization conditions as in panels a and b, respectively. In panel e the ratio ρ is plotted for both the SFG signal obtained at different ω_1 (black solid dots) and the SHG signal pumped by different ω_2 (blue open dots). The error bars show the standard deviation of four independent measurements.

DOI: 10.1021/jp511058b
J. Phys. Chem. B 2015, 119, 3356−3365

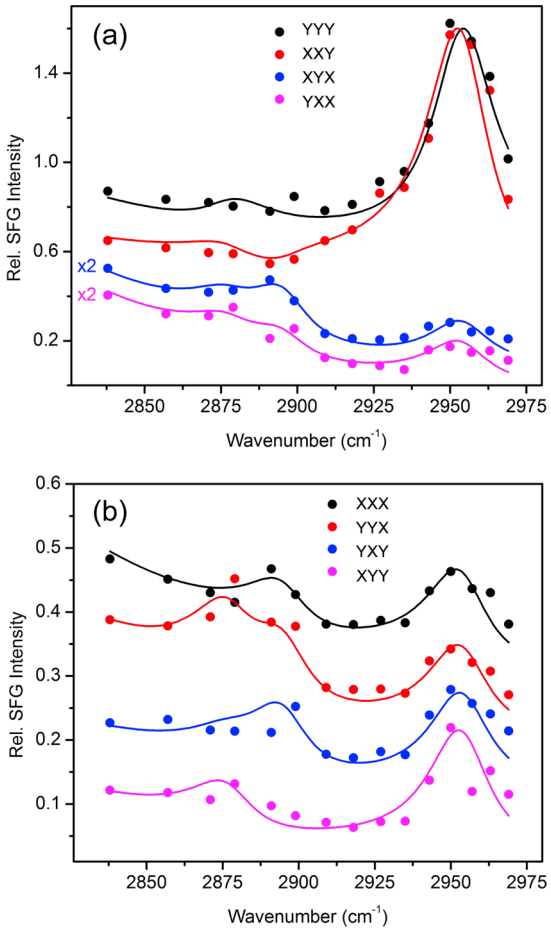

Figure 5. Spectral dependence of selected tensor elements in the CH-stretching region of the vibrational spectrum. (a) Spectral dependence of the *YYY*, *XXY*, *XYX*, and *YXX* tensor elements. (b) Spectral dependence of the *XXX*, *YYX*, *YXY*, and *XYY* tensor elements. The long axis of collagen was aligned along the *Y*-axis ($\phi = 0$) in all cases. Curves are vertically offset for clarity.

range. Assuming C_{2v} symmetry for the methylene mode, the tensor elements can be related to the molecular hyperpolarizabilities. Within the limits of the bond polarizability derivative model,[34,35] we expect no strong symmetric vibration to appear in the $\chi^{(2)}_{yxx}$ and $\chi^{(2)}_{xyx}$ elements, whereas the contribution of the symmetric mode in $\chi^{(2)}_{xxy}$ is expected to be strong.[5] We indeed observed this trend for the 2954 cm^{-1} resonance, which is in concert with previous assignments of this band to a symmetric stretching vibration.[16,27] Because the vibrational energy of this resonance seems rather high for a CH_2-symmetric stretch, it has been suggested that the observed band may correspond to the shifted Fermi-resonance between the stretching modes and bending mode overtones of methylene.[27]

The main features of the spectra can be reproduced by fitting the data to three Lorentzian lines. Besides the main band at 2954 cm^{-1}, weaker bands are observed at 2896 and 2877 cm^{-1}. Details on the fit are given in the Supporting Information. The two weaker bands at lower energy are most evident in the $\chi^{(2)}_{YXX}$ and $\chi^{(2)}_{XYX}$ spectra. In the current model, this contribution is not likely to stem from a symmetric methylene mode of fibrillar collagen. To investigate the origin of this weaker resonance, the spectra of the $\chi^{(2)}_{XXX}$, $\chi^{(2)}_{XYY}$, $\chi^{(2)}_{YYX}$, and $\chi^{(2)}_{YXY}$ elements were recorded as well, shown in Figure 5b. Note that the cylindrical symmetry of aligned collagen ($\phi = 0$) precludes a strong contribution from these elements. Although the spectral features shown in Figure 5b are indeed much weaker than the strong peak of the $\chi^{(2)}_{YYY}$ and $\chi^{(2)}_{XXY}$ elements, clear signatures with vibrational energies identical to the energies found in Figure 5a can be identified. The clear presence of the lower energy peaks in elements other than $\chi^{(2)}_{YYY}$ and $\chi^{(2)}_{XXY}$ suggests that these modes may be attributed to tissue components other than aligned collagen. To gain more insight into the differences between the spectral regions near 2885 and 2950 cm^{-1}, we studied their relative contributions as a function of the orientation of the collagen fibers, which we will discuss next.

3.3. Orientation Dependence of the Collagen SFG Signal. The dependence of the SFG signal as a function of the fiber orientation can reveal important information about the relative contributions of the nonvanishing tensor elements at a given vibrational energy. In Figure 6, we show the SFG signal measured for the $\chi^{(2)}_{YYY}$, $\chi^{(2)}_{XXY}$, $\chi^{(2)}_{XYY}$, and $\chi^{(2)}_{YXY}$ experimental configurations as a function of the orientation angle ϕ of the collagen fibers. The functional dependence of the SFG signal under these conditions is given in the Supporting Information. The first column in Figure 6 shows the signal measured at $\omega_1 =$ 2949 cm^{-1}, representative for the spectral region near 2950 cm^{-1}. At this vibrational energy, the signal is well described by the four elements $\chi^{(2)}_{yyy}$, $\chi^{(2)}_{xxy}$, $\chi^{(2)}_{xyx}$, and $\chi^{(2)}_{yxx}$, whereas other elements are negligibly small. It can be seen that the *YYY* and *XXY* signals show a similar $\cos^3\phi$ dependence. This behavior is in accordance with the strong contribution of the $\chi^{(2)}_{yyy}$ and $\chi^{(2)}_{xxy}$ elements in this region, and the weaker amplitudes of the $\chi^{(2)}_{yxx}$ and $\chi^{(2)}_{xyx}$ elements. The *XYY* and *YXY* signals, on the other hand, are correspondingly weaker, and mimic characteristic four-leaf clover patterns. A global fit at the 2949 cm^{-1} vibrational energy reproduces the main trends and correlates the relative magnitudes of the different tensor elements, as shown in Table 1. Based on the fitting result, the value for $|\chi^{(2)}_{yyy}/\chi^{(2)}_{yxx}|^2$ is 16, consistent with the measured ratio $\rho \approx 15$.

The 2882 cm^{-1} signal, representative of the 2885 cm^{-1} spectral region, is shown in the second column of Figure 6. The signal exhibits a remarkably different polarization dependence. The SFG signal of this band is maximized when the collagen fibers are oriented along the *X*-axis. For this orientation, the signal in the *YYY* and *XXY* configurations is expected to be zero for a system with cylindrical symmetry. To describe the observed anisotropy, it is necessary to include the other four elements $\chi^{(2)}_{xxx}$, $\chi^{(2)}_{yyx}$, $\chi^{(2)}_{yxy}$, and $\chi^{(2)}_{xyy}$. The fit indicates that the $\chi^{(2)}_{xxx}$ and $\chi^{(2)}_{yyx}$ elements carry significant weight, elements that explicitly vanish for rod-like molecules with rotational symmetry along the *y*-axis. Therefore, it is unlikely that the bands at this vibrational energy originate from aligned collagen. This observation provides further evidence that a tissue structure other than collagen fibers may be responsible for the signal found at this lower vibrational energy.

The last column in Figure 6 summarizes the fiber orientation dependence of the SFG signal at an off-resonance frequency (2845 cm^{-1}). Compared to the SFG signal at 2882 and 2949 cm^{-1}, the off-resonance signal displays a more isotropic character as a function of fiber orientation. Maximum signal in the *YYY* configuration is still seen when the fiber is aligned with the *Y*-axis, as expected for a cylindrically symmetric system, but the orientation dependence is remarkably less compared to the situation at 2949 cm^{-1}. Part of the observed anisotropy can be explained by the presence of a fluorescence background that is assumed to be isotropic. However, after

DOI: 10.1021/jp511058b
J. Phys. Chem. B 2015, 119, 3356−3365

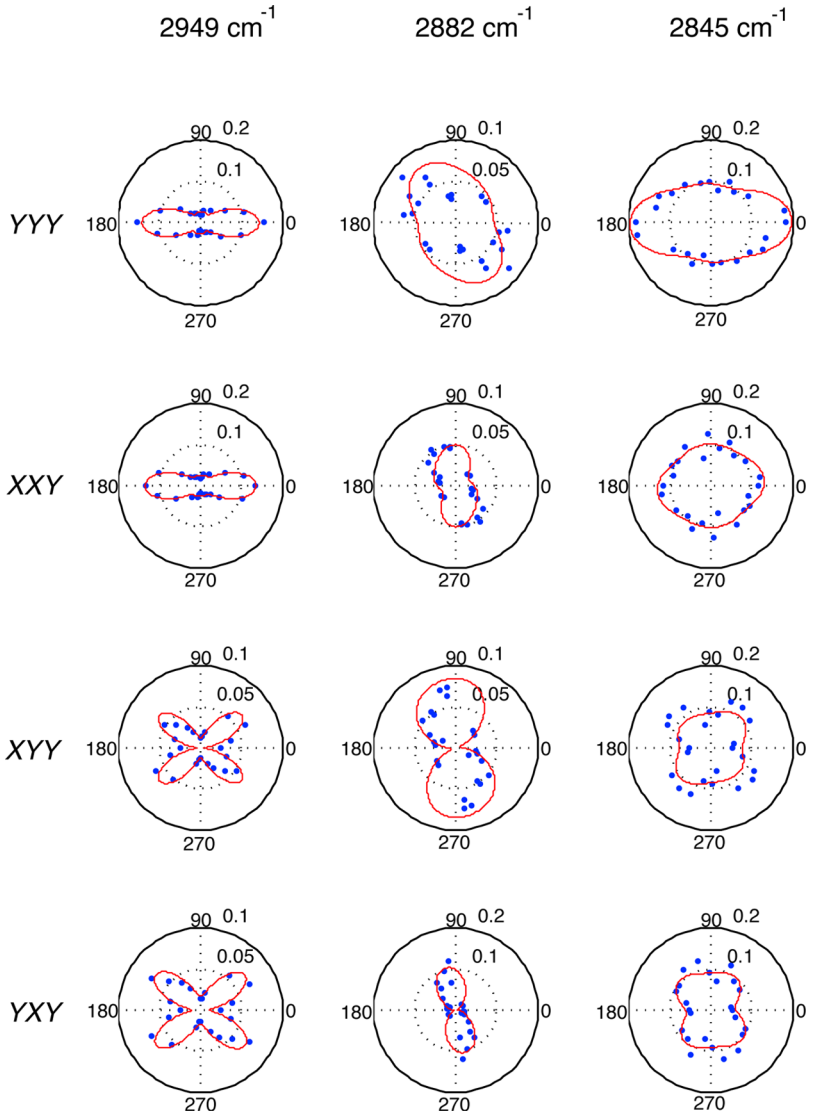

Figure 6. Anisotropy of the SFG tensor elements (*YYY*), (*XXY*), (*XYY*), and (*YXY*) as a function of fiber orientation angle ϕ. The first, second, and third columns show the results obtained at 2949, 2882, and 2845 cm^{-1}, respectively. Dots show the experimental data points and red line shows fits obtained with the model presented in the Appendix. The graphs in each column are fitted simultaneously.

Table 1. Amplitudes of Tensor Elements Relative to the Value of $\chi^{(2)}_{yyy}$ Measured at 2949 cm^{-1}[a]

	2949 cm^{-1}	2882 cm^{-1}	2845 cm^{-1}
yyy	1.00 ± 0.07	0.06 ± 0.09	0.51 ± 0.04
xxy	−0.97 ± 0.08	0.15 ± 0.10	0.28 ± 0.07
xyx	0.24 ± 0.15	0.60 ± 0.05	0.28 ± 0.06
yxx	0.25 ± 0.15	−0.55 ± 0.05	0.15 ± 0.08
xxx	0.01 ± 0.19	0.29 ± 0.08	0.06 ± 0.11
yyx	0.01 ± 0.18	0.35 ± 0.07	0.02 ± 0.10
yxy	0.00 ± 0.11	−0.07 ± 0.09	−0.06 ± 0.07
xyy	0.00 ± 0.11	0.14 ± 0.08	0.01 ± 0.08

[a]The values with the indicated margins correspond to the 95% confidence interval of the least-squares fitting procedure.

accounting for the background, it is clear that the SFG signal in the *YYY* configuration is no longer carried predominantly by the $\chi^{(2)}_{yyy}$ component as other elements gain in relative importance, rendering the observed ϕ-dependence overall less anisotropic. See Table 1 for the fitting results. These measurements confirm that the ϕ-dependent anisotropy is much more significant near the ∼2950 cm^{-1} resonance than at off-resonance frequencies.

Figure 6 shows that the ϕ-dependence of the *YYY* and *XXY* signals is virtually identical. We thus expect that the ratio $\chi^{(2)}_{XXY}/\chi^{(2)}_{YYY}$ is fairly insensitive to the ϕ-orientation of the fiber. Figure 7 shows an image where the *YYY* (green) and *XXY* (red) signals at 2950 cm^{-1} are overlapped. The image shows marked variations between the *YYY* and *XXY* signals that are local in nature. Since *YYY* and *XXY* transform similarly in ϕ, these local variations are not expected to depend on variations in ϕ, but rather on variations in the tilt angle θ of the fiber out of the *XY* plane. If the fibers exhibit a small tilt angle θ out of the *XY* plane, more elements are needed to describe the measured signal from the collagen fibers, including chiral tensor elements, which affect the $\chi^{(2)}_{XXY}/\chi^{(2)}_{YYY}$ ratio (see the Appendix). In short, besides providing information about fiber orientation in the lateral plane, SFG signals can also retrieve information on the tilt angle θ, namely, through examination of the ratios of selected $\chi^{(2)}$ tensor elements.

DOI: 10.1021/jp511058b
J. Phys. Chem. B 2015, 119, 3356−3365

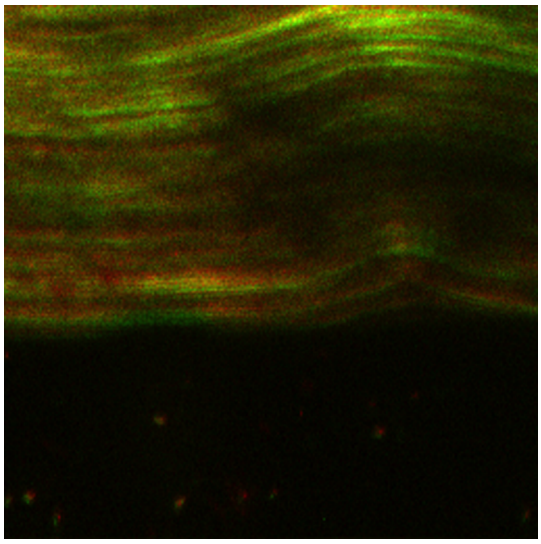

Figure 7. Overlay of $\chi^{(2)}_{YYY}$ (green) and $\chi^{(2)}_{XXY}$ (red) images taken at 2949 cm^{-1} and $\phi = 0$. Note that the *YYY* and *XXY* signals are not identical throughout the entire image. Differences between the *YYY* and *XXY* signals can be related to out-of-plane orientation of the collagen fibers.

4. DISCUSSION

Point-scanning SFG microscopy is a chemically selective imaging technique that adds a new contrast mechanism to the nonlinear optical microscope. Because SFG signal generation relies on noncentrosymmetry in the sample, the technique shares many of its imaging properties with SHG microscopy, a technique that is widely used for the visualization of collagen in tissues. To evaluate the potential of vibrationally resonant SFG microscopy, it is important to compare several of its capabilities with conventional SHG microscopy. It is clear that the ability to tune into specific vibrational resonances provides a more direct way to study molecular compounds in tissues. Yet, it is important to delineate what meaningful imaging parameters can be attained with SFG microscopy that are, in practice, difficult to access with nonresonant SHG contrast. In this work, we highlight some of the additional benefits that SFG microscopy offers over SHG imaging by studying a prime target in biological imaging: collagen I fibers. In particular, we advanced point-scanning SFG microscopy to include polarization-sensitive detection capabilities and showed that resolving individual tensor elements of the second-order susceptibility can offer greater insight in the molecular properties of the sample.

The objective of the current study is not to unravel the molecular origin of the optical nonlinearity of collagen I fibrils per se, but rather to investigate the enhanced imaging properties of SFG imaging over SHG microscopy. One of the key observations in this work is that the contrast of $\chi^{(2)}$-sensitive microscopy is significantly improved when tuned into a molecular resonance. The 2954 cm^{-1} resonance, which can be attributed to a symmetric methylene vibration of collagen, provides strong SFG signals with minimal background. Moreover, the resonant signal is highly anisotropic as a function of the fiber orientation angle ϕ, much more so than the nonresonant $\chi^{(2)}$ signal at 2845 cm^{-1}, giving rise to collagen images with sharper contrast.

Polarization-resolved imaging enabled us to investigate the origin of the sharper contrast, by studying the spectral and ϕ-dependence of individual tensor elements. We found that the 2954 cm^{-1} resonance selectively enhances the $\chi^{(2)}_{yyy}$ and $\chi^{(2)}_{xxy}$ elements, whereas the amplitude of other elements remains close to the levels of the nonresonant background. This selective enhancement partially explains why the $\chi^{(2)}_{yyy}/\chi^{(2)}_{yxx}$ anisotropy ratio and thus the corresponding ρ value is significantly higher in on-resonance SFG relative to off-resonance signals, yielding higher contrast images from aligned collagen fibers. The improved ratio is confirmed in both polarization-resolved spectral measurements and the polarization-resolved anisotropy measurements.

In addition to the strong 2954 cm^{-1} resonance, weaker peaks in the 2885 cm^{-1} range were identified. Our combined spectral- and orientation-dependent analysis revealed that, under the assumption that the collagen fiber has $C_{\infty v}$ symmetry, the lower energy bands may not originate from collagen itself. On the basis of this observation, the contribution of other tissue components cannot be excluded. Although it is not clear which tissue constituents could give rise to the weak signal in the 2885 cm^{-1} range, the ability to identify the tentative presence of $\chi^{(2)}$-active tissue structures is an example of the added benefits of polarization-resolved SFG studies. Another example of the deeper level of analysis offered by SFG imaging is given in Figure 7, where the ability to resolve the *YYY* and *XXY* response will make it possible to retrieve information on the fiber's out-of-plane orientation from a 2D image.

In general, polarization-resolved SFG offers two main advantages over nonresonant SHG microscopy. First, tuning into specific molecular resonances avoids ambiguity regarding the origin of the $\chi^{(2)}$-dependent signal. It is not always clear which portions of the molecule give rise to the $\chi^{(2)}$ response when operating under nonresonant conditions. In SHG microscopy studies of collagen fibers, which are typically performed with 800 nm laser pulses derived from Ti:sapphire lasers, no particular molecular resonances are excited. Hence, the resulting SHG signal may contain contributions from the wings of various off-resonant modes. It is likely that the signal is dominated by electronic transitions in the amino-acid backbone, which are generally strong and are found relatively close to the frequency of the second harmonic.[31] Others have suggested that off-resonant contributions from vibrational transitions may also play a role, although their frequencies are more remote and the corresponding transition amplitudes are lower.[25,27] In SFG microscopy, the nonresonant contributions are inferior relative to the resonant contribution when tuning into the 2954 cm^{-1} methylene mode of collagen. Because it is clear which part of the molecule produces the detected SFG signal, it is easier to draw conclusions regarding structure and orientation of the molecule.

Second, the ability to spectrally resolve the nonlinear response from the sample offers an opportunity to distinguish different contributors to the signal. In this study we found spectral components that appear distinct from the expected response from collagen I, indicating that there may be a weak contribution from other tissue components to the signal. This type of information cannot be retrieved from nonresonant SHG imaging studies, because SHG is not capable of spectrally distinguishing the different signal contributions. Spectrally resolved SFG microscopy thus provides discovery-based imaging capabilities not available through SHG microscopy.

Third, polarization-sensitive SFG measurements allow inspection of individual tensor elements. In this study, we examined a total of 8 different $\chi^{(2)}$ tensor elements. Because the ω_1 and ω_2 fields are the same for the SHG process, only a select

DOI: 10.1021/jp511058b
J. Phys. Chem. B 2015, 119, 3356−3365

few tensor elements can be studied in SHG microscopy. In particular, in studies concerned with characterizing chiral contributions, which explicitly rely on tensor elements with ω_1 and ω_2 fields of different polarization, the additional flexibility of polarization-resolved SFG microscopy offers tangible benefits.

The additional capabilities of SFG microscopy relative to SHG microscopy listed above are not limited to the study of collagen I. SFG imaging is also useful for studying the structural properties of $\chi^{(2)}$-active assemblies such as acto-myosin complexes, cellulose fibers, and microcrystallites of chiral biomolecules.[14] For instance, SFG microscopy makes it possible to distinguish individual microcrystallites in a larger ensemble of crystalline molecular structures based on the spectroscopic properties of the material.

Polarization-sensitive detection is common practice in SFG spectroscopy, which has proven a powerful analytical method for studying molecules at planar interfaces. In this work, we import some of these spectroscopic capabilities into the realm of point-scanning microscopy. Compared to macroscopic SFG spectroscopy, the collinear beam arrangement in point-scanning SFG microscopy offers advantages and disadvantages. In SFG spectroscopy of planar samples, the polarization orientation of the participating fields is typically characterized relative to the plane of incidence at the surface, assigning the fields either as s-polarized (parallel to surface) or p-polarized (in the plane of incidence). The different polarization combinations allow interrogation of $\chi^{(2)}_{ijk}$ where the indices span all Cartesian coordinates (x, y, z). In collinear SFG microscopy, however, field components along z are negligible, which implies that tensor elements with z indices cannot be independently examined. On the other hand, when $\phi = 0$ and $\chi^{(2)}_{IJK} = \chi^{(2)}_{ijk}$, the x,y indices in collinear SFG microscopy can be independently controlled and provide direct access to individual tensor elements, rather than to a combination of tensor elements such as is the case in $\chi^{(2)}_{ppp}$ spectroscopy measurements of a rotationally isotropic achiral interface. It should be noted, however, that the collinear excitation configuration in point-scanning SFG is fundamentally different from the geometry commonly used in SFG spectroscopy of interfaces, and that a description of the measured collinear SFG signal cannot be directly ported from established SFG models found in the literature. Rather, in terms of spatial coherence, phase-matching, and signal emission patterns, point-scanning SFG microscopy shares most of its imaging properties with SHG microscopy.

5. CONCLUSION

In this work, we have advanced point-scanning SFG microscopy to include polarization-sensitive detection. This capability enables direct access to selected elements of the second-order susceptibility, which facilitates the study of molecular orientation in microstructured samples. We have applied this new capability to the study of collagen I fibers in tissues. A spectral and orientation analysis of the collagen fiber revealed that the $\chi^{(2)}_{yyy}$ and $\chi^{(2)}_{xxy}$ tensor elements of collagen are selectively enhanced over nonresonant signal components. The SFG signal derived from these elements is highly anisotropic as a function of fiber orientation, and gives rise to image contrast that is notably higher than what is observed in nonresonant SHG measurements. The improved contrast and the ability to tune into specific molecular resonances make point-scanning SFG microscopy an attractive addition to the family of nonlinear optical imaging techniques.

APPENDIX

The second-order polarization that generates the SFG signal is related to the electric field of the excitation beams by

$$P^{(2)}_I(\omega_3) = \chi^{(2)}_{IJK} E_J(\omega_2) E_K(\omega_1) \tag{A1}$$

The nonlinear susceptibility measured in the laboratory frame is related to the nonlinear susceptibility of the collagen fiber in the following way:

$$\chi^{(2)}_{IJK} = \sum_{ijk} R_{Ii} R_{Jj} R_{Kk} \chi^{(2)}_{ijk} \tag{A2}$$

where the rotation matrix $\mathbf{R}$ is used to relate the coordinates (i, j, k = x, y, z) of the collagen fiber to the coordinates of the laboratory frame (I, J, K = X, Y, Z). The relation between the two frames can be described by the two angles (ϕ, θ), as sketched in Figure 2. We generally assume that, in the rat tail tendon tissue, the collagen fibers are predominantly aligned in the lateral plane, i.e., $\theta \approx 0$. Under these conditions, the measured tensor element $\chi^{(2)}_{IJK}$ is related to the fiber nonlinear susceptibility by the collagen orientation angle ϕ. If $\phi = 0$, the measured tensor element is directly related to the corresponding tensor element of the molecule, $\chi^{(2)}_{IJK} = \chi^{(2)}_{ijk}$. However, if the orientation angle ϕ deviates from zero, the measured response is a combination of all eight nonzero tensor elements that are relevant in the current experimental configuration ($\chi^{(2)}_{yyy}$, $\chi^{(2)}_{yxx}$, $\chi^{(2)}_{xxy}$, $\chi^{(2)}_{xyx}$, $\chi^{(2)}_{xxx}$, $\chi^{(2)}_{xyy}$, $\chi^{(2)}_{yyx}$, and $\chi^{(2)}_{yxy}$). Note that the latter four elements cannot be ascribed to a cylindrically symmetric system aligned along the y-axis but may arise because of other structures in the tissue. The $\chi^{(2)}_{yzz}$, $\chi^{(2)}_{zzy}$, $\chi^{(2)}_{zyz}$, $\chi^{(2)}_{zyy}$, $\chi^{(2)}_{yyz}$, and $\chi^{(2)}_{yzy}$ elements do not contribute to $\chi^{(2)}_{IJK}$ when (I, J) = (X, Y) and θ = 0. The measured tensor elements are related to these eight nonzero elements as follows:

$$\chi^{(2)}_{YYY} = \chi^{(2)}_{yyy}\cos^3\phi + \{\chi^{(2)}_{yxx} + \chi^{(2)}_{xxy} + \chi^{(2)}_{xyx}\}\sin^2\phi\cos\phi + \chi^{(2)}_{xxx}\sin^3\phi + \{\chi^{(2)}_{xyy} + \chi^{(2)}_{yyx} + \chi^{(2)}_{yxy}\}\sin\phi\cos^2\phi \tag{A3}$$

$$\chi^{(2)}_{XXY} = \chi^{(2)}_{xxy}\cos^3\phi + \{\chi^{(2)}_{yyy} - \chi^{(2)}_{yxx} - \chi^{(2)}_{xyx}\}\sin^2\phi\cos\phi + \chi^{(2)}_{yyx}\sin^3\phi + \{\chi^{(2)}_{xxx} - \chi^{(2)}_{xyy} - \chi^{(2)}_{yxy}\}\sin\phi\cos^2\phi \tag{A4}$$

$$\chi^{(2)}_{XYY} = \chi^{(2)}_{xyy}\cos^3\phi + \{\chi^{(2)}_{xxx} - \chi^{(2)}_{yyx} - \chi^{(2)}_{yxy}\}\sin^2\phi\cos\phi - \chi^{(2)}_{yxx}\sin^3\phi - \{\chi^{(2)}_{yyy} - \chi^{(2)}_{xxy} - \chi^{(2)}_{xyx}\}\sin\phi\cos^2\phi \tag{A5}$$

$$\chi^{(2)}_{YXY} = \chi^{(2)}_{yxy}\cos^3\phi + \{\chi^{(2)}_{xxx} - \chi^{(2)}_{xyy} - \chi^{(2)}_{yyx}\}\sin^2\phi\cos\phi - \chi^{(2)}_{xyx}\sin^3\phi - \{\chi^{(2)}_{yyy} - \chi^{(2)}_{yxx} - \chi^{(2)}_{xxy}\}\sin\phi\cos^2\phi \tag{A6}$$

Although the approximation $\theta \approx 0$ is reasonable, in some cases, small variations in θ can lead to additional differences in the measured tensor elements. We consider next the effect of variations in both ϕ and θ on the elements $\chi^{(2)}_{YYY}$ and $\chi^{(2)}_{XXY}$. To simplify the analysis, we consider only the nonzero elements of collagen in the limit of cylindrical symmetry, including both achiral and chiral components:

DOI: 10.1021/jp511058b
J. Phys. Chem. B 2015, 119, 3356−3365

$$\chi^{(2)}_{YYY} = \chi^{(2)}_{yyy}\cos^3\phi\cos^3\theta + \{\chi^{(2)}_{yxx} + \chi^{(2)}_{xxy} + \chi^{(2)}_{xyx}\}\sin^2\phi\cos\phi\cos\theta + \{\chi^{(2)}_{yzz} + \chi^{(2)}_{zzy} + \chi^{(2)}_{zyz}\}\cos^3\phi\sin^2\theta\cos\theta \quad \text{(A7)}$$

$$\chi^{(2)}_{XXY} = \chi^{(2)}_{xxy}\cos^3\phi\cos\theta + \{\chi^{(2)}_{yyy}\cos^2\theta - \chi^{(2)}_{yxx} - \chi^{(2)}_{xyx}\}\sin^2\phi\cos\phi\cos\theta + \{\chi^{(2)}_{yzz} + \chi^{(2)}_{zzy} + \chi^{(2)}_{zyz}\}\sin^2\phi\cos\phi\sin^2\theta\cos\theta + \{\chi^{(2)}_{yxz} + \chi^{(2)}_{xyz}\}\sin\phi\cos^2\phi\sin\theta\cos\theta - \{\chi^{(2)}_{zyx} + \chi^{(2)}_{yzx}\}\sin^3\phi\sin\theta\cos\theta \quad \text{(A8)}$$

Because of the tilt angle θ, there are additional differences between $\chi^{(2)}_{YYY}$ and $\chi^{(2)}_{XXY}$. In particular, all the elements in the (YYY) measurement are achiral, whereas the last term in the (XXY) measurement contains chiral elements.

■ ASSOCIATED CONTENT

Supporting Information

Details on the polarization analysis and the fitting procedure. This material is available free of charge via the Internet at http://pubs.acs.org.

■ AUTHOR INFORMATION

Corresponding Author

*E-mail: epotma@uci.edu. Tel: 949-824-9942.

Notes

The authors declare no competing financial interest.

■ ACKNOWLEDGMENTS

We thank Prof. James Jester for providing the hawk cornea sample. This work was supported by the National Science Foundation (NSF), Grants CHE-0847097 to E.O.P. and 1414466 and 1310693 to N.-H.G. J.H. acknowledges support from the NSF IGERT program in biophotonics at UCI (NSF-DGE-1144901).

■ REFERENCES

(1) Shen, Y. R. Surface Properties Probed by Second-Harmonic and Sum-Frequency Generation. *Nature* **1989**, *337*, 519−525.

(2) Eisenthal, K. B. Equilibrium and Dynamic processes at Interfaces by Second Harmonic and Sum Frequency Generation. *Annu. Rev. Phys. Chem.* **1992**, *43*, 627−661.

(3) Shen, Y. R. Surfaces Probed by Nonlinear Optics. *Surf. Sci.* **1994**, *299*, 551−562.

(4) Eisenthal, K. B. Liquid Interfaces Probed by Second-Harmonic and Sum-Frequency Spectroscopy. *Chem. Rev.* **1996**, *96* (4), 1343−1360.

(5) Wang, H. F.; Gan, W.; Lu, R.; Rao, Y.; Wu, B. H. Quantitative Spectral and Orientational Analysis in Surface Sum Frequency Generation Vibrational Spectroscopy. *Int. Rev. Phys. Chem.* **2005**, *24:2*, 191−226.

(6) Brasselet, S. Polarization-Resolved Nonlinear Microscopy: Application to Structural and Biological Imaging. *Adv. Opt. Photonics* **2011**, *3*, 205−271.

(7) Cimatu, K. A.; Baldelli, S. Chemical Microscopy of Surfaces by Sum Frequency Generation Imaging. *J. Phys. Chem. C* **2009**, *113*, 16575−16588.

(8) Flörsheimer, M.; Brillert, C.; Fuchs, H. Chemical Imaging of Interfaces by Sum Frequency Microscopy. *Langmuir* **1999**, *15* (17), 5437−5439.

(9) Hieu, H. C.; Tuan, N. A.; Li, H.; Miyauchi, Y.; Mizutani, G. Sum Frequency Generation Microscopy Study of Cellulose Fibers. *Appl. Spectrosc.* **2011**, *65*, 1254−1259.

(10) Hoffmann, D. M. P.; Kuhnke, K.; Kern, K. Sum-Frequency Generation Microscope for Opaque and Reflecting Samples. *Rev. Sci. Instrum.* **2002**, *73* (9), 3221−3226.

(11) Inoue, K.; Fujii, M.; Sakai, M. Development of a Non-Scanning Vibrational Sum-Frequency Generation Detected Infrared Super-Resolution Microscope and Its Application to Biological Cells. *Appl. Spectrosc.* **2010**, *64*, 275−281.

(12) Hernandez, M.; Chinwangso, P.; Cimatu, K.; Srisombat, L.; Lee, T. R.; Baldelli, S. Chemical Imaging and Distribution Analysis of Mono-, Bi-, and Tridentate Alkanethiol Self-Assembled Monolayers on Gold by Sum Frequency Generation Imaging Microscopy. *J. Phys. Chem. C* **2011**, *115* (11), 4688−4895.

(13) Mizutani, G.; Koyama, T.; Tomizawa, S.; Sano, H. Distiniction Between Some Saccharides in Scattered Optical Sum Frequency Intenisty Images. *Spectrochim. Acta, Part A* **2005**, *62*, 845−849.

(14) Chung, C. Y.; Boik, J. C.; Potma, E. O. Biomolecular Imaging with Coherent Nonlinear Vibrational Microscopy. *Annu. Rev. Anal. Chem.* **2013**, *64*, 77−99.

(15) Li, H.; Miyauchi, Y.; Tuan, N. A.; Mizutani, G.; Koyano, M. Optical sum frequency generation image of rice grains. *J. Biomat. Nanobiotechnol.* **2012**, *3* (2A), 286−291.

(16) Han, Y.; Raghunathan, V.; Feng, R.-r.; Maekawa, H.; Chung, C.-Y.; Feng, Y.; Potma, E. O.; Ge, N.-H. Mapping Molecular Orientation with Phase Sensitive Vibrationally Resonant Sum-Frequency Generation Microscopy. *J. Phys. Chem. B* **2013**, *117* (20), 6149−6156.

(17) Yue, S. H.; Slipchenko, M. N.; Cheng, J. X. Multimodal Nonlinear Optical Microscopy. *Laser Photon. Rev.* **2011**, *5* (4), 496−512.

(18) Raghunathan, V.; Han, Y.; Korth, O.; Ge, N.-H.; Potma, E. O. Rapid Vibrational Imaging With Sum Frequency Generation Microscopy. *Opt. Lett.* **2011**, *36* (19), 3891−3893.

(19) Millard, A. C.; Campagnola, P. J.; Mohler, W.; Lewis, A.; Loew, L. M. Second Harmonic Imaging Microscopy. *Methods Enzymol.* **2003**, *361*, 47−69.

(20) Zoumi, A.; Yeh, A.; Tromberg, B. J. Imaging Cells and Extracellular Matrix In Vivo by Using Second-Harmonic Generation and Two-Photon Excited Fluorescence. *Proc. Natl. Acad. Sci. U.S.A.* **2002**, *99* (17), 11014−11019.

(21) Campagnola, P. J.; Loew, L. M. Second-Harmonic Imaging Microscopy for Visualizing Biomolecular Arrays in Cells, Tissues and Organisms. *Nat. Biotechnol.* **2003**, *21* (11), 1356−1360.

(22) Sivaguru, M.; Durgam, S.; Ambekar, R.; Luedtke, D.; Fried, G.; Stewart, A.; Toussaint, K. C. Quantitative Analysis of Collagen Fiber Organization in Injured Tendons Using Fourier Transform-Second Harmonic Generation Imaging. *Opt. Express* **2010**, *18* (24), 24983−24993.

(23) Cicchi, R.; Vogler, N.; Kapsokalyvas, D.; Dietzek, B.; Popp, J.; Pavone, F. S. From Molecular Structure to Tissue Architecture: Collagen Organization Probed by SHG Microscopy. *J. Biophotonics* **2013**, *6* (2), 129−142.

(24) Psilodimitrakopoulos, S.; Santos, S. I. C. O.; Amat-Roldan, I.; Thayil, A. K. N.; Artigas, D.; Loza-Alvarez, P. In Vivo, Pixel-Resolution Mapping of Thick Filaments' Orientation in Nonfibrilar Muscle Using Polarization-Sensitive Second Harmonic Generation Microscopy. *J. Biomed. Opt.* **2009**, *14* (1), 014001−1−014001−11.

(25) Su, P.-J.; Chen, W.-L.; Chen, Y.-F.; Dong, C.-Y. Determination of Collagen Nanostructure from Second-Order Susceptibility Tensor Analysis. *Biophys. J.* **2011**, *100* (8), 2053−2062.

(26) Tuer, A. E.; Krouglov, S.; Prent, N.; Cisek, R.; Sandkuijl, D.; Yasufuku, K.; Wilson, B. C.; Barzda, V. Nonlinear Optical Properties of Type I Collagen Fibers Studied by Polarization Dependent Second Harmonic Generation Microscopy. *J. Phys. Chem. B* **2011**, *115* (44), 12759−12769.

(27) Rocha-Mendoza, I.; Yankelevich, D. R.; Wang, M.; Reiser, K. M.; Frank, C. W.; Knoesen, A. Sum Frequency Vibrational

DOI: 10.1021/jp511058b
J. Phys. Chem. B 2015, 119, 3356−3365

Spectroscopy: The Molecular Origins of the Optical Second-Order Nonlinearity of Collagen. *Biophys. J.* **2007**, *93*, 4433−4444.
(28) Diesner, M.-O.; Welle, A.; Kazanci, M.; Kaiser, P.; Spatz, J.; Koelsch, P. In Vitro Observation of Dynamic Ordering Processes in the Extracellular Matrix of Living, Adherent Cells. *Biointerphases* **2011**, *6* (4), 171−179.
(29) Reiser, K. M.; McCourt, A. B.; Yankelevich, D. R.; Knoesen, A. Structural Origins of Chiral Second-Order Optical Nonlinearity in Collagen: Amide I Band. *Biophys. J.* **2012**, *103* (10), 2177−2186.
(30) Johansson, P. K.; Koelsch, P. Vibrational Sum-Frequency Scattering for Detailed Studies of Collagen Fibers in Aqueous Environments. *J. Am. Chem. Soc.* **2014**, *136* (39), 13598−13601.
(31) Perry, J. M.; Moad, A. J.; Begue, N. J.; Wampler, R. D.; Simpson, G. J. Electronic and Vibrational Second-Order Nonlinear Optical Properties of Protein Secondary Structural Motifs. *J. Phys. Chem. B* **2005**, *109* (42), 20009−20026.
(32) Richards, B.; Wolf, E. Electromagnetic Diffraction in Optical Systems II: Structure of the Image Field in an Aplanatic System. *Proc. R. Soc. London, Ser. A* **1959**, *253*, 358−379.
(33) Chen, X.; Nadiarynkh, O.; Plotnikov, S.; Campagnola, P. J. Second Harmonic Generation Microscopy for QuantitativeAnalysis of Collagen Fibrillar Structure. *Nature Protocols* **2012**, *7*, 654−669.
(34) Hirose, C.; Akamatsu, N.; Domen, K. Formulas for the Analysis of Surface Sum−Frequency Generation Spectrum by CH stretching Modes of Methyl and Methylene Groups. *J. Chem. Phys.* **1992**, *96* (2), 997−1004.
(35) Hirose, C.; Yamamoto, H.; Akamatsu, N.; Domen, K. Orientation Analysis by Simulation of Vibrational Sum Frequency Generation Spectrum: CH Stretching Bands of the Methyl Group. *J. Phys. Chem.* **1993**, *97* (39), 10064−10069.

DOI: 10.1021/jp511058b
J. Phys. Chem. B 2015, 119, 3356−3365